Contents lists available at ScienceDirect

Composites Science and Technology

journal homepage: http://www.elsevier.com/locate/compscitech

Multifunctional composite combining chitosan microspheres for drug delivery embedded in shape memory polyester-urethane matrix

Monika Bil [a],[1],[*], Piotr Mrówka [b],[c], Dorota Kołbuk [d], Wojciech Święszkowski [a]

[a] Faculty of Materials Science and Engineering, Warsaw University of Technology, 141 Wołoska Street, Warsaw, 02-507, Poland
[b] Department of Biophysics and Human Physiology, Medical University of Warsaw, 5 Chalubinskiego Street, 02-004, Warsaw, Poland
[c] Institute of Hematology and Transfusion Medicine, 14 Indiry Gandhi Str., 02-776, Warsaw, Poland
[d] Institute of Fundamental Technological Research, Polish Academy of Sciences, 5B Pawińskiego Street, 02-106, Warsaw, Poland

A B S T R A C T

Multifunctional composite biomaterials (3b-PU/CH_M) consisting of chitosan microspheres (CH-M) that provide drug release functionality and crosslinked polyester-urethane (3b-PU) matrix responsible for shape memory properties were designed. A series of 3b-PU/CH_M bio-composites with varying weight fraction of CH-M (2.5, 5, and 10 wt %) embedded into 3b-PU matrix were synthesized. The ATR-FTIR confirmed the presence of covalent bonds between 3b-PU matrix and CH-M as well as enhanced hydrogen bonds interaction within bio-composites matrix in comparison to neat 3b-PU. It was found that CH-M had not impaired the shape memory properties of 3b-PU matrix and even slightly improved the shape recovery (R_r %). The R_r value increased to 100% for 3b-PU/CH 2.5% M and 3b-PU/CH 5% M after the third thermo-mechanical cycle. Moreover, the transition temperature (T_{trans}) of shape recovery tailored to 30 °C by the chemical composition of the 3b-PU network was not affected by CH-M. Effectiveness of the application of the composites as a controlled drug delivery system at various pH conditions was confirmed in an in vitro release study of ciprofloxacin hydrochloride (Cpx-HCl) used as a model drug. In vitro biocompatibility studies revealed that the materials do not alter the cells' ability to proliferate and differentiate.

1. Introduction

Biomaterials science has developed side by side with novel technologies in regenerative medicine based on patient specific tissue engineering products and tailored implants or stimuli-responsive devices, that are expected to allow more effective and less invasive surgical procedures. Along with novel strategies in medicine and pharmacy, the requirements for the functionality of implants become more complex. Therefore, an emerging trend in biomaterials design is integrating various functionalities, including shape memory, biodegradability, and drug delivery, in a single material [1–3].

Multifunctionality may be accomplished by adding a particular component that contributes to a new independent function that occurs at a predetermined time or where one function follows the previous one sequentially [2]. The major challenge in designing such a material is ensuring that the new function does not interfere with the other ones. This goal can be achieved by designing composite materials, combining

natural and synthetic polymers, that provide more options for modulating the molecular structure and phase morphology as compared to a homogenous material. The benefits of such an approach have been already confirmed and verified showing improved surface biocompatibility, mechanical performance or biological activity of the implants, drug delivery systems, and medical devices utilizing composite materials [1,4–6].

Development of multifunctional composites based on shape memory polymers (SMPs) is a promising strategy leading to obtaining the next generation of smart drug delivery systems and tissue engineering scaffolds [2,4,7]. SMPs are a class of smart materials, which can revert from temporary to permanent shape when exposed to suitable external stimuli. The macromolecule network of the temperature responsive SMPs consists of at least two components: switching domains and permanent netpoints. Switching domains may undergo thermally reversible changes of softening and hardening, triggered by temperature changes above the glass transition temperature T_g or the crystalline phase

melting temperature (T_m). Permanent netpoints are covalent bonds or physical netpoints (microcrystalline or hard domains) associated with a high thermal transition temperature (T_m or T_g). When designing a polymer network of temperature responsive SMPs for biomedical applications, many specific features must be considered, such as the transformation temperature (T_{trans}) of the switching segment near the 37 °C, biodegradation ability *in vivo*, a lack of toxicity or appropriate mechanical properties [7,8]. Among various polymers, polyurethanes are extensively investigated as a polymer matrix with shape memory performance for various medical applications due to their confirmed biocompatibility [9–12]. Although polyurethane properties and biological functionality can be adjusted in the broad range by modification of synthesis parameters and substrates properties [8–10], further enhancement of shape memory and biocompatibility can be achieved through incorporation of chitin or chitosan unities [12]. Chitosan is an example of a natural biopolymer, which offers various advantages for biomedical applications such as biodegradability, biocompatibility, and antibacterial activity, what makes it a very attractive material for design of drug and gene delivery carriers [13,14], tissue engineering scaffolds, and wound healing implants [15,16]. Therefore, chitin or chitosan were used not only as a specific chain extender or PU macromolecular unit [12,16] but also as a filler at PU/chitosan composites added in the form of flakes, nanocrystals or fibers [12,17,18].

The main objective of the previously reported study was to analyze the effect of chitin or chitosan incorporation on shape memory capability, mechanical properties, or biocompatibility of the biocomposites in comparison to the pure polymer. The purpose of this study was to develop a multifunctional material, where chitosan was not only used as a renewable nanofiller for reinforcement or improvement of existing functions but also as a component that supplies the final material system in drug delivery capability as additional functionality. Therefore, according to our best knowledge, chitosan was for the first time incorporated to polyester urethane matrix in the form of microspheres that were used as a drug carrier. To understand the structure – property – function correlations, the chemical structure, shape memory, thermomechanical properties, and drug delivery capability were evaluated and discussed. Additionally, a preliminary study of cell response and toxicity was performed.

2. Experimental section

2.1. Materials

Chitosan from shrimp shells with deacetylation ≥75% (Sigma Aldrich) was purified by filtration. ε-Caprolactone (CL) (Sigma Aldrich) was purified by distillation over calcium hydride under reduced pressure. D, L-lactide monomers (LA), glycolide (GA) (PURASORB®, Corbion, The Netherlands) purchased from BIOMATPOL (Poland) were recrystallized from anhydrous ethyl acetate and dried under vacuum before use. Ciprofloxacin hydrochloride (Cpx-HCl) was purchased from Alfa Aesar. 1,6-hexamethylene diisocyanate (HDI) and Tin (II)-2-ethylhexanoate (SnOct2), trimethylolpropane (TMP), triphosphate pentasodium (TPP), glutaraldehyde solution 50% and Span 80 were purchased from Sigma Aldrich. Commercially available methanol, n-hexane, and ethyl ether were purchased from Avantor Performance Materials (Poland) and used as received. N, *N*-dimethylformamide (DMF) and 1,4-butanediol (BD) were dried with a molecular sieve before use.

2.2. Composite synthesis

CH-M were prepared according to the emulsification/chemical crosslinking method published by Szymanska et al. [19]. The exact information regarding synthesis of CH-M is provided in Supplementary Information. Three branched PCL polyols (3*b*-PCL-OH) and two branched 2b-PDLG-OH polyols with monomer ratio of D-lactide to glycolide of 70:30, terminated with hydroxyl groups, were synthesized by ring opening polymerization [10]. Polyols molecular weights are presented in Table 1S (Supplementary Information). 3b-PU/CH_M composites were synthesized by a one-step polymerization method. The polyols (ratio of 3*b*-PCL-OH to 2*b*-PDLG-OH of 70:30 by weight) were blended under vacuum for 2 h at 120 °C under continuous stirring using mechanical stirrer. After cooling to 50 °C nitrogen was connected to the reaction flask and chitosan microspheres previously dispersed in 20 mL of THF (2.5%, 5% or 10 wt%) were inserted into the reaction mixture and stirred for 15 min. Next, HDI and the catalyst were dropped into the solution, mixed for 5 min, cast to Teflon molds, placed in a vacuum oven and degassed by applying three vacuum/nitrogen refill cycles, and cured for the next 24 h at 80 °C. The isocyanate index (NCO equivalents/polyol equivalents x 100) was 102. The polymers films were washed in ethanol and dried under vacuum at 50 °C for 3 days.

2.3. Structure and morphology characterization

Infrared spectra of the chitosan microspheres and chitosan/polyurethane composites were collected by a Fourier transform infrared spectrophotometer (Thermo Fisher Scientific model Nicolet 6700). Measurements were carried out using the attenuated total reflectance (ATR) technique. Each sample was scanned 64 times at a resolution of 4 cm^{-1} over the frequency range of 4000–400 cm^{-1}. DSC measurements were performed with differential scanning calorimeter DSCQ2000 (TA Instrument). All measurements were performed in a nitrogen atmosphere using standard crimped aluminum pans. Samples, were scanned at a heating rate of 10 °C min^{-1} and a cooling rate of 5 °C min^{-1} at the temperature range of −85 °C ÷ 200 °C using a heat/cool/heat cycle. Tm and Tg temperatures were determined from the second heating scan. Wide Angle X-ray Scattering (WAXS) technique was applied for the detection of the crystalline structure of the samples before shape memory programming process. WAXS measurements were performed using Bruker D8 Discover (Germany) according previously used methodology [20]. Peaks on WAXS radial profiles from crystal and amorphous phases were deconvoluted using Pearson VII and Gauss function, respectively. Crystallinity of 3b-PU was determined as ratio of the sum of the area of crystal peaks from 3b-PU and the total profile area (crystal and amorphous) scattered on 3b-PU." Methodology was used previously for other compositions [20]. Tensile strengths (Rm) and Young's moduli (E) were measured using an INSTRON 5943 (sample size 5 mm × 25 mm x 0.5 mm). The gauge section between the clamps was set at 10 mm. The mean values of 3 measurements ± standard deviations were reported. The initial gauge length L0 was 10 mm, the strain rate was 5 mm/min. The morphology of the microspheres and the brittle fracture surfaces of the composites were analyzed by SEM microscopy (the Phenom proX desktop scanning electron microscope (PhenomWorld. The Netherlands) at 10 kV. The surfaces for the observation were prepared after brittle-fracture of the biocomposite films previously frozen in the liquid nitrogen. All samples were sputter coated with 7 nm gold (Leica EM SCD500, Leica Microsystems) under 25 mA and 10-2 mbar.

2.4. Programming of shape memory

Programming of shape memory properties was performed on dynamic mechanical analyzer DMA Q800 (TA Instruments) under strain rate mode. The sample was pre-heated to 40 °C, and then a strain deformation was applied until 50% (ε_m). The strain was held constant while the sample was cooled down to 5 °C and kept at this temperature for 30 min. The strain (ε_u) was then released and the sample was heated up to 37 °C, while the length recovery (ε_p) was monitored. This heat-cool-heat procedure was cycled three times. Shape recovery ratio (R_r) and shape fixing ratio (R_f) were calculated using the following equations:

$$R_r = \frac{\varepsilon_m(N) - \varepsilon_p(N)}{\varepsilon_m(N) - \varepsilon_p(N-1)} \times 100, \quad R_f = \frac{\varepsilon_u(N)}{\varepsilon_{m(N)}} \times 100, \text{respectively}$$

where: ε_m (N) - maximum strain, ε_p-strain after recovery, ε_u (N) is the sample's strain immediately following unloading.

2.5. In vitro release study

Ciprofloxacin hydrochloride Cpx-HCl release study was performed in phosphate buffered saline (pH 7.4 or pH 6.4). The CH-M 50 mg or chitosan composites films were placed in vials filled with 5 mL of a release medium. The vials were kept at 37 °C with rotational mixing of 50 rpm. At specified time points, the release medium was taken out and fresh release medium was added between each time point. The drug concentration was analyzed with an UV/VIS (Evolution 60, Thermo Fischer Scientific) spectrophotometer at the wavelength of 272 nm, based on the previously prepared calibration curve. The mean values of 3 measurements ± standard deviations were reported. Cumulative release was based on the initial amount of drug entrapped in the CH-M.

2.6. Biocompatibility evaluation

Human osteosarcoma MG-63 cells (Lonza) were maintained according to the manufacturer's protocol (DMEM supplemented with 10% heat-inactivated fetal bovine serum (FBS) (Lonza) and antibiotic-antimycotic solution (Sigma), 37 °C, 5% CO_2, in a humidified atmosphere). Cytostatic and/or cytotoxic effects of compounds released to the medium from materials during degradation were assessed using CV staining performed as described before [10]. Briefly, after 48 h of incubation with supernatants from degradation studies, cells were stained with 0.5% CV. Absorbed dye was dissolved in 1% SDS and measured at 595 nm wavelength using an ELISA reader (FLUOstar OPTIMA). The results of cells survival are expressed as a mean compared to control ± SD. The XTT assay based on the ability of mitochondrial dehydrogenase enzymes of living cells to convert the XTT substrate (2.3-bis (2-methoxy-4-nitro-5-sulfophenyl)-5 [(phenyloamino)carboxyl]-2H-tetrazolium hydroxide) was used to determine cells viability after according producer protocoland as described previously [10]. The absorbance of color product was measured using ELISA reader (FLUOstar OPTIMA) at a wavelength of 450 nm. For quantification of the relative cell number, Quant-iT™ PicoGreen™ dsDNA Assay was used as described before [21] according to the manufacturer's instructions (ThermoFisher Scientific). The osteogenic potential of the MG63 cells was evaluated using ALP activity assay [21], following the colorimetric procedure provided in Phosphatases, Alkaline, Acid, Prostatic Acid kit (Sigma). Absorbance of the final product was measured at the excitation filter of 405 nm, using a ELISA reader. The data were presented either in percentages of untreated control or with reference to cells cultured on PS (polystyrene of culture dishes), with mean ± S.D. Mean values calculated from at least 4 independent measurements were used for the statistical analysis. One-way ANOVA and Tukey's multiple comparisons *post hoc* test was used for the statistical analysis (GraphPad Prism 6), with the significance level set at $p < 0.05$ or lower (as indicated in figures captions).

3. Results and discussion

3.1. Structure and morphology

The smart bio-composites consisting of chitosan microspheres (CH-M) which act as drug delivery carriers and a biodegradable thermoresponsive 3b-PU matrix that provides a shape memory function were synthesized by *in situ* polymerization. The effectiveness of the multifunctional biocomposites based on SMP is controlled by the composite structure [22]; therefore, the structure – property – functions correlations were analyzed at various structural levels. To evaluate the influence of CH-M on shape memory capability, three compositions were prepared consisting of 2.5, 5, and 10 (wt.%) CH-M embedded into 3b-PU

matrix assigned as 3b-PU/CH 2.5% M, 3b-PU/CH 5% M, and 3b-PU/CH 10% M, respectively. CH-M were synthesized with a double crosslinking TPP/GL system (Fig. 1S–A Supplementary Information) to guarantee the stability of the obtained microspheres in the synthesis environment. ATR-FTIR analysis (Fig. 2) revealed that CH-M spectrum contains two new bands appeared at 1648 cm^{-1} and 1559 cm^{-1} (Fig. 2) formed due to crosslinking reactions of chitosan (Fig. 1S–A Supplementary Information). The band at 1559 cm^{-1} can be assigned to antisymmetric deformation N–H vibrations in NH3+ ions [23]; whereas, the peak around 1648 cm^{-1} could be the result of an overlapping vibration of the C=N bond of azomethine group formed during the reaction of chitosan with GL on an already existing band associated with C=O stretching of amide I of the chitosan acetyl group [24].

The stability of the CH-M during 3b-PU/CH-M synthesis (Fig. 1A) and thus effectiveness of the double TPP/GL crosslinking system was further confirmed through SEM analysis of the fractured surfaces of the biocomposites. The SEM images presented in Fig. 2S (Supplementary Information) confirmed that CH-M are uniformly dispersed within 3b-PU matrix. The SEM micrographs taken at higher magnification (Fig. 1 B, C and D), indicated that the quasi-spherical shape of CH-M (Fig. 1S -D) was well preserved and the microspheres are well bonded to the polymer matrix. The SEM analysis confirmed that CH-M microspheres were not disintegrated during synthesis (Fig. 1B–D, Fig. 2 S) and therefore, can preserve its function as a drug carrier.

The covalently crosslinked PU matrix was obtained through the reaction of hydroxyl groups of the three branched PCL-triol and PDLG-diol or chitosan with isocyanate groups leading to the urethane bond formation (Fig. 1A), what was confirmed by the ATR-FTIR analysis (Fig. 2). FTIR spectra of various types of bio-composites show bands characteristic of the urethane group, i.e. hydrogen bonded N–H stretching vibration of the urethane group at 3370-3384 cm^{-1}, amide II bond associated with the combined N–H deformation and C–N stretching vibrations present at 1525 -1531 cm^{-1} and peak at 1237-1239 cm^{-1} assigned to coupled C–N and C–O stretching vibrations. Strong peak at 1721-1723 cm^{-1} region is assigned to the carbonyl group of ester and urethane bonds [25,26]. When comparing a spectrum of neat 3b-PU with 3b-PU/CH bio-composites spectra, new bands appeared around 1625 cm^{-1} arising from an ordered hydrogen-bonded carbonyl group in the urea band [27] and at 1568 cm^{-1}, that can be assigned to amide II vibration in urea groups [28]. The urea linkages could be formed due to reaction between the amine chitosan group and isocyanate, what was also reported by other authors [17,18]. Since the hydrogen bonds act as physical cross-links and thus provide the driving force for shape recovery additional analysis of the FTIR spectra was performed to evaluate the effect of CH-M on hydrogen bonds formation. The FTIR spectra revealed that peak at 3383 cm^{-1} attributed to the vibration of N–H bond shifts towards lower wavenumbers after incorporation of 2.5 and 5 (wt.%) of chitosan microspheres, suggesting that in these two types of composites more N–H groups of urethane units are involved in hydrogen bonding than in neat 3b-PU and 3b-PU/CH 10% M composite. The same trend was also observed at the carbonyl region, where a slight shift towards the lower wavenumbers was observed for 3b-PU/CH 2.5% and 3b-PU/CH 5%M. After deconvolution of C=O bands and Gaussian-/Lorentzian fitting, additional bands appeared (Supplementary Information Table 2S, Fig. 3S). In the case of neat 3b-PU, non-associated urethane carbonyl at 1723 cm^{-1} and hydrogen bonded urethane carbonyl at 1700 cm^{-1} were present. For 3b-PU/CH-M biocomposites, an additional peak at 1682-1688 cm^{-1} appeared that can indicate either the presence of well-ordered or crystalline, hydrogen bonded urethane groups formed due to a reaction of active groups of CH-M and 3b-PU or it could be derived from urea units formed due to a reaction of amine groups of chitosan and isocyanate [29].

The band, typical for hydrogen bonded carbonyl urea units, appeared at 1655 cm^{-1} for 3b-PU/CH 5% M [30]. To evaluate quantitatively the percent of the hydrogen bonded carbonyl groups of the urethane units, the hydrogen bonding carbonyl index (R) was calculated
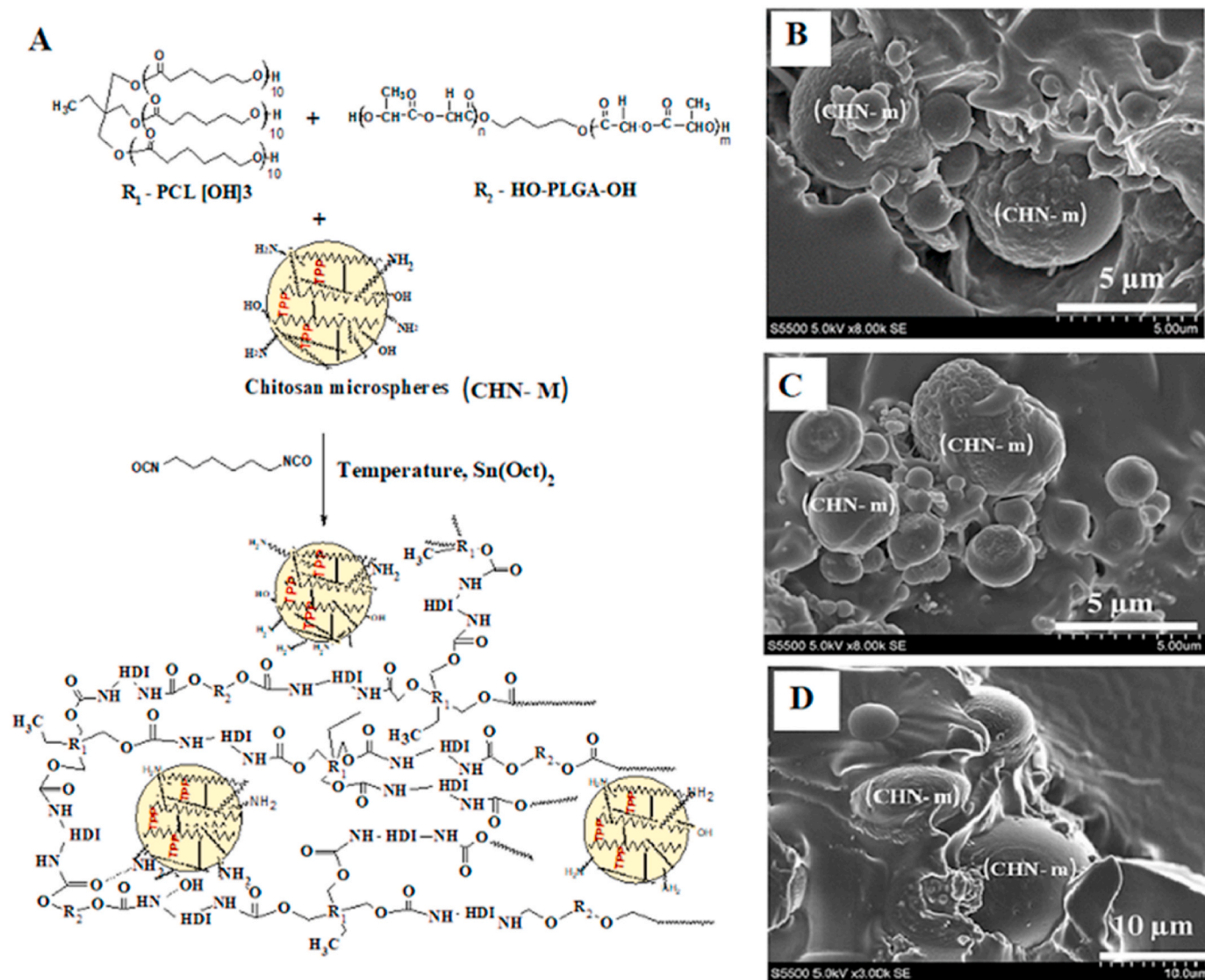
Fig. 1. Chemical structure and morphology of CH-M/PU; A) reaction scheme and chemical structure of 3b-PU/CH-M biocomposites; SEM micrographs presenting the freeze-fractured surfaces of B) 3b-PU/CH- 2.5% M C) 3b-PU/CH 5% M and D) 3b-PU/CH 10% M, respectively.

(Table 2S Supplementary Information). These calculations revealed that the R index increased after incorporation of CH-M from 16% for 3b-PU to 27% for the bio-composite with 2.5% of CH-M and to 21% and 22% for 3b-PU/CH 5% M, and 3b-PU/CH 10%, respectively. The ATR-FTIR analysis confirmed that the incorporation of CH-M results in formation of the additional urea covalent bonds and enhances the hydrogen bonds interactions which may act as permanent netpoints able to improve shape memory properties [10,22,31].

In the case of SMP associated with melting/crystallization transition, crystallinity degree is crucial for shape memory efficiency as crystallites fix the temporary shape. The crystallinity degree was evaluated by a WAXS analysis presented in Fig. 3. Several diffraction peaks attributed to an amorphous and crystal structure of 3b-PU and CH-M appeared at the radial profiles of 3b-PU/CH 2.5% M, 3b-PU/CH 5% M, and 3b-PU/CH 10% M and pure 3b-PU. Deconvolution of the experimental profile of 3b-PU revealed the following peaks: 15.715.5 deg, 21.34 deg, 23.723,6 deg, and 27.829,7 deg corresponding to (001), (110)/(111), (200)/(201), and (210)/(201) lattice planes, respectively, and two an amorphous halos with a maximum at $2\theta = 16$ deg and at $2\theta = 23$ deg, what is in line with other authors [32].

The same angular positions of the peaks were observed for composites as for pure 3b-PU what proves that CH-M did not change the crystal unit cell (Fig. 3A). There were no additional peaks characteristic of chitosan crystals observed by other authors [33] at 10.2deg. and 20.0deg. CH-M indicated only an amorphous halo with a maximum at $2\theta = 12.7$ deg. Contrarily, the crystallinity degree estimated from the deconvolution of the WAXS radial profiles, increased from 31% for neat 3b-PU to 51% for 3b-PU/CH 2.5% M. Next, the decreasing of the crystallinity was observed with a higher fraction of CH-M to 41% and substantial reduction to 9% for 3b-PU/CH 5% M and 3b-PU/CH 10% M, respectively (Fig. 4B). A small fraction of microspheres (2.5–5%) enhanced crystallization, acting as a nucleation centre what was also reported by other authors [18]. However, incorporation of 10% microspheres blocked 3b-PU chains mobility, reorganization and flexibility and enhance separation of 3b-PU chains thus hindering crystallization [34]. This was further substantiated through the DSC studies which revealed increasing of Tg with increasing amount of CH-M (Fig. 4) what indicates on lower chains mobility. Additionally, the melting enthalpy (ΔH_m) and the crystallization enthalpy (ΔH_c) reported in Table 3S (Supplementary information) followed the same trend with the increasing fraction of CH-M as the changes of the crystallinity observed by WAXS.

DSC heating scans presented in Fig. 4 confirmed the presence of only one endothermic transition around 30 °C associated with the melting of
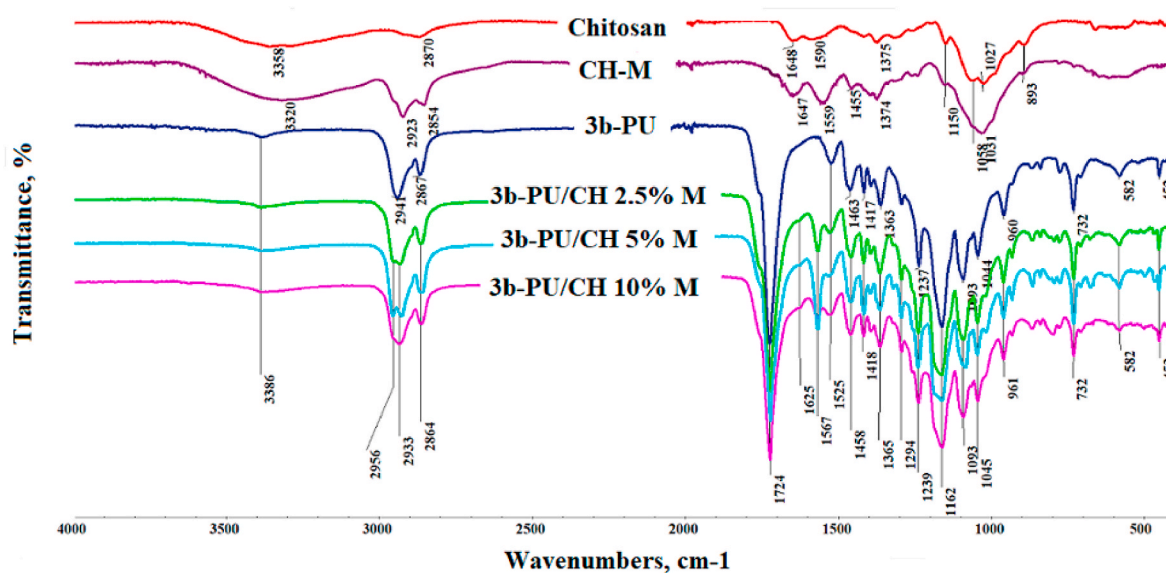
Fig. 2. FTIR-ATR spectra of chitosan, CH-M microspheres, neat 3b-PU and bio-composites with CH-M.
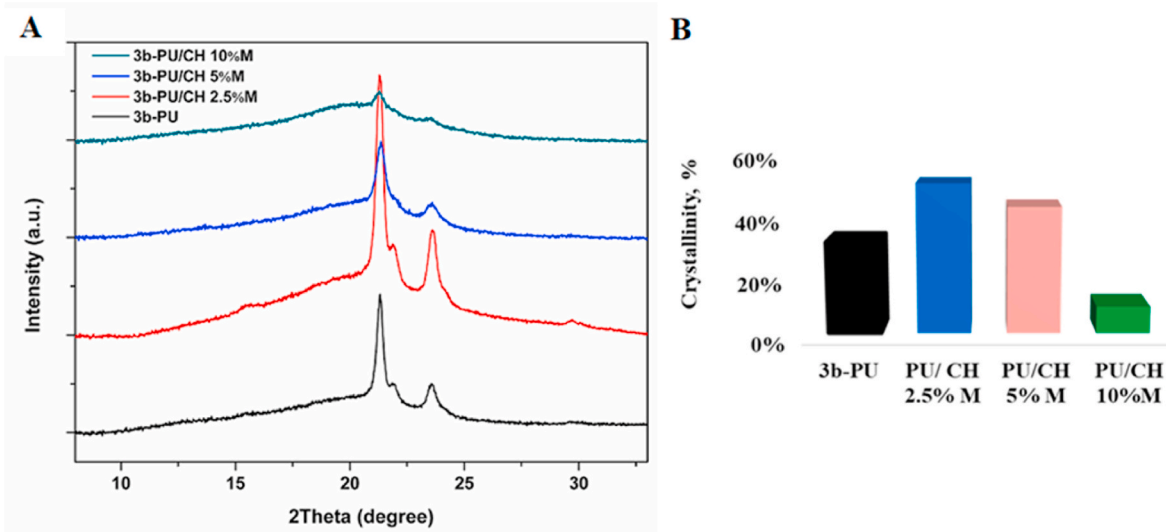

Fig. 3. WAXS radial profiles of CH-M/3b-PU biocomposites A) Crystallinity degree in the function of CH-M content B).

o-PCL crystalline phase. The position of the peak did not change with the increasing amount of CH-M and the melting temperature (T_m) of the soft/switching phase remained nearly constant (Fig. 4). Consequently, it can be concluded that (T_{trans}), associated with the melting point of PCL semi-crystalline units, is not influenced by CH-M and can be modulated independently only by changes of the chemical structure of the 3b-PU matrix. Further, these results suggest that human body temperature triggers shape recovery of 3b-PU/CH-M composite after implantation what guarantees convenient utilization of the thermoresponsive 3b-PU/CH-M composites in medicine without the need to apply external heating and thus eliminating the risk of injury. On the other hand, melting peaks become broader with the increasing fraction of CH-M in 3b-PU matrix (Fig. 4), indicating a broader crystal size distribution and broader melting -transition temperature span.

3.2. Mechanical properties

The tensile test results of the neat 3b-PU and composites presented in Table 1, confirmed that the observed microstructural changes resulted in

the increasing of Young modulus E of the bio-composites. The E for 3b-PU was found to be 78 MPa, and increased up to the maximum value of 130 MPa for 3b-PU/CH 2.5% M, and next, some decrease of E was observed with an increasing loading of CH-M to 101 MPa and 77 MPa for 3b-Pu/CH 5 wt% M, and 3b-PU/CH 10 wt% M, respectively (Table 1). These results are consistent with the crystallinity degree evaluation (Table 1) as the crystalline phase acts as a specific reinforcement leading to increased composite toughness in the elastic region [19,20]. In the case of R_m, only for 10 wt% of CH-M, an increase of the ultimate tensile strength was observed in comparison to neat 3b-PU up to 5.6 MPa, whereas for bio-composites with a lower content of CH-M, R_m was not changed and remained approx. 4 MPa (Table 1).

3.3. Shape memory effect

The shape recovery and fixity behavior of 3b-PU and 3b-PU/CH biocomposites were programmed during thermo-mechanical cyclic tensile test, which is illustrated in Fig. 5 A, B. The collected data were used for calculating shape fixity (R_f) and shape recovery ratio (R_r)
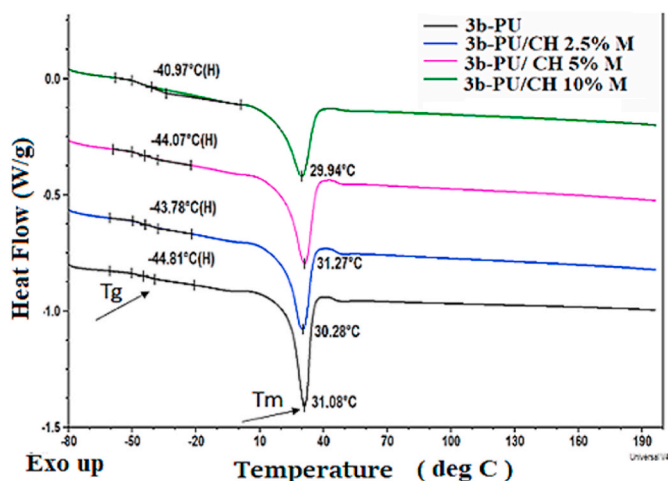
Fig. 4. DSC thermograms of 3b-PU/CH M biocomposites (the second heating scan).

Table 1
Tensile test results of 3b-PU and 3b-PU/CH M bio-composites.

	3b-PU	3b-PU/CH 2.5% M	3b-PU/CH 5% M	3b-PU/CH 10% M
Rm, [MPa]	4.5 ± 0.1	4.1 ± 0.5	4.5 ± 0.9	5.7 ± 1.2
E, [MPa]	78 ± 8	130 ± 27	101 ± 22	77 ± 16

values, presented in Fig. 5 C, D, respectively. Fig. 5 C depicts that all samples exhibit excellent shape fixity irrespective of the amount of CH-M added. It is demonstrated that R_{f_1} was in the range of 95–99% for the first thermo-mechanical cycle. For the third cycle a slight increasing of

R_{f_3} was observed and finally R_{f_3} reached values from 97% for 3b-PU/CH 10% M to 100% for the other bio-composites and neat polymer. Slightly lower value of R_f observed for 3b-PU/CH- 10% M may be due to lower crystallization degree evaluated by WAXS. Additionally, the broader transition temperature range observed in DSC could be the reason of less stable or incomplete shape fixing and slower shape recovery as the sample needs more time for crystallization in comparison to the composites with a narrow melting point range. Similarly, the recovery ratio R_r increased with the number of thermo-mechanical tensile cycles from the range of 63–85% in the first cycle to 97–100% in the third cycle (Fig. 5 D). Moreover, influence of CH-M content on the R_r ratio was more evident in the first cycle. Specifically, R_{r_1} increased from 75% for 3b-PU to 86% for 3b-PU/CH-2,5% M due to presence of the highest amount of hydrogen bonds (Table 2S) that enabled fast shape recovery. Subsequently, decreasing of R_r with higher content of CH-M was observed with the lowest value of 63% for the 3b-PU/CH-10% M composite. On the other hand, for the third thermo-mechanical cycle, R_r values increased to 99% for 3b-PU/CH-10% M and to 100% for 3b-PU/CH-2,5% M and 3b-PU/CH-5% M whereas the lowest value was detected for 3b-PU polymer. The lower values of R_r for the first thermo-mechanical cycle were also reported in the previous study [31]. This relates to plastic and nonreversible deformation that occurs during the first thermo-mechanical cycle but diminishes in the subsequent thermo-mechanical cycles what results in the improvement of R_r. Summarizing, it could be concluded that the incorporation of CH-M did not impaired shape memory properties of 3b-PU matrix. Furthermore, additional covalent urea bonds and hydrogen bonds that were formed as a result of the incorporation of CH-M that act as permanent netpoints responsible for the original shape recovery [31], even slightly improved the shape recovery ratio in comparison to 3b-PU matrix. Also nearly constant shape fixity for all of the samples allow us to conclude that incorporation of CH-M as the component that provide new function to the final composite, did not diminished the shape memory behavior that is mainly provided by the polymer matrix and thus confirms the idea of
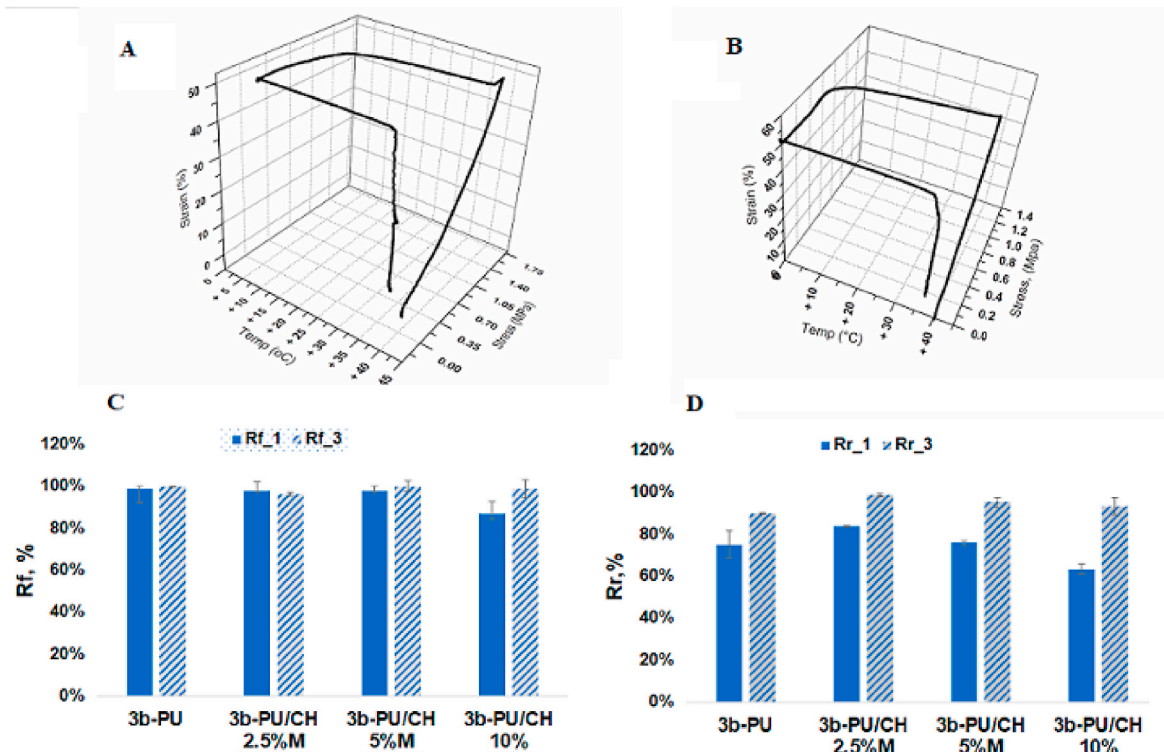

Fig. 5. Representative images of the three-dimensional diagram of thermo-mechanical programming cycle for A) 3b-PU and B) 3b-PU/CH 10% M. Values of shape fixity ratio C) (R_f %) and D) shape recovery ratio (R_r %) calculated after the first and the third thermo-mechanical programming cycle.

creating a multifunctional system by combining these two components.

3.4. Drug release

The *in vitro* release study of the model drug Cpx-HCl were performed to study the effectiveness of drug delivery from CH-M entrapped in 3b-PU matrix and to evaluate the performance of the developed multifunctional system in terms of second functionality. The 3b-PU/CH 10% M biocomposites with the theoretically highest amount of drug were chosen to allow the most accurate measurements. The results are presented in Fig. 6. As shown in Fig. 6, the kinetics of Cpx-HCl release from biocomposite is much lower, without a significant burst release stage in comparison to the release profile from microspheres. In the case of chitosan microspheres, two-stage release profile was observed, with an initial burst release that reached 25% after 24 h. Next, the sustained release profile was observed in both PBS solutions with a slightly higher amount of the drug released in acidic PBS (pH 6.4) up to 46% of the loaded Cpx-HCl after 17 days. The obtained results indicate that the slightly acidic conditions used in the experiment affected the chitosan morphology. Moreover, Cpx-HCl has a higher solubility in acidic conditions that resulted in an increased kinetic release. However, the incorporation of the chitosan drug carrier to the 3b-PU matrix provides additional protection of microspheres and no significant differences in the drug release profile were observed in various pH conditions.

To better understand the mechanism that governs drug release, the results of the *in vitro* release were applied in different mathematical models, interpreted graphically, and evaluated by correlation coefficient (R^2) shown in Table 2. In the case of CH-M, the best fitting was found for the Korsmeyer-Peppas release model with R^2 coefficient 0.944 and 0.930 for pH 6.4 and 7.4, respectively. Diffusion exponent (n) value used to characterize the release mechanism is 0.35 ± 0.01 (pH 6.4) and 0.32 ± 0.01 (pH 7.4). These values are in good agreement with the values reported by Ritger et al. [35] for microparticles drug delivery system with size distribution and indicate the Fickian diffusion mechanism. The multifunctional drug release system 3b-PU/CH 10% M tested in acidic and neutral media follows the Korsmeyer-Peppas model with n values of 0.28 ± 0.01 and 0.35 ± 0.05, respectively (Table 2). For a bio-composite, a very good linear fitting of Cpx -HCl release data was observed for the Higuchi model what indicates a diffusion-controlled mechanism [36]. However, the degradation of the polymer matrix as well as chitosan microspheres should be considered as a driving force of the release profile, especially in the later stage of degradation [37].

To summarize the effectiveness of a multifunctional system, it can be concluded that CH-M after incorporation to 3b-PU matrix, sustain their ability for long-term delivery of the drug. The ability of 3b-PU/CH-M bio-composite to deliver anti-inflammatory drugs locally in controlled
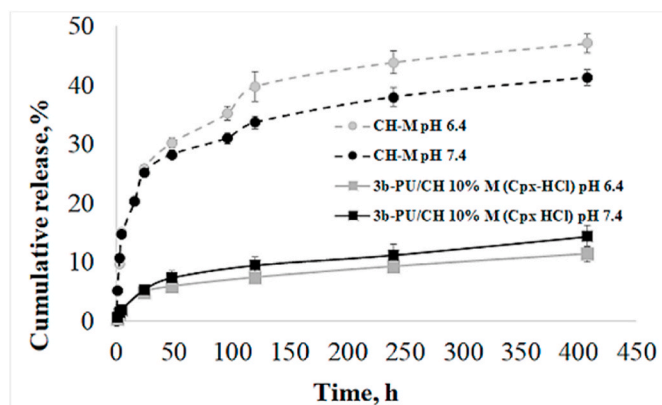

Fig. 6. In vitro release profiles of Cpx-HCl from chitosan microspheres and 3b-PU/CH 10%M casting films in various pH PBS solution. Mean±SD of 3 samples per each time point are shown.

Table 2
Correlation coefficient R^2 from *in vitro* release data of Cpx-HCl for different release kinetics models.

Sample	Zero order	1st order	Higuchi	Korsmeyer- Peppas	
	Regression co-efficient R^2 value				(n)
CH-M – pH 6.4	$0.658 \pm$ 0.02	$0.723 \pm$ 0.02	$0.867 \pm$ 0.01	$0.944 \pm$ 0.01	$0.35 \pm$ 0.01
CH-M – pH 7.4	$0.611 \pm$ 0.01	$0.709 \pm$ 0.01	$0.885 \pm$ 0.02	$0.930 \pm$ 0.01	$0.32 \pm$ 0.01
3b-PU/CH 10%M pH 6.4	$0.801 \pm$ 0.03	$0.808 \pm$ 0.01	$0.948 \pm$ 0.02	$0.992 \pm$ 0.02	$0.28 \pm$ 0.01
3b-PU/CH 10% M pH 7.4	$0.813 \pm$ 0.02	$0.824 \pm$ 0.01	$0.959 \pm$ 0.01	$0.971 \pm$ 0.03	$0.35 \pm$ 0.05

manner could address problems associated for example with orthopedic implants such as inflammations, infections and thus could prolong implantable device function or support traditional antibiotic therapy in the implantation site and eliminate side effects by minimizing systemic exposure.

3.5. Biocompatibility study

For the biocompatibility studies, the 3b-PU/CH 2.5%M composite material has been selected for its best shape memory properties. 3b-PU without microspheres served as control.

To test if the materials release any cytotoxic compounds to the growth medium, material pucks were placed in wells of a 96-well culture plate with 200 μl DMEM medium. After 72 h, the material-conditioned media were transferred to MG-63 cells. Both the viability (XTT) (Fig. 7A) and the number (CV) (Fig. 7B) of cells were at the same level as in the control group. The experiment indicates that the analyzed materials do not release any toxic substances and are safe for the cellular microenvironment. Next, we seeded MG-63 cells directly on the materials. Material modifications did not affect the viability – XTT assay (Fig. 7 C) nor proliferation – PicoGreen® assay (Fig. 7D) of cells cultured on the surface of the samples. To investigate the osteogenic potential of the cells, ALP activity was measured after 7 days of culture on the materials (Fig. 7 E). ALP activity on both tested materials was also similar. As both materials equally allow osteogenic differentiation of MG-63 cells supporting normal growth and differentiation thus we conclude that addition of CH-M is safe and should not impair normal bone cells function.

4. Conclusions

Multifunctional chitosan – polyurethane composites that integrate shape memory properties, drug delivery ability, and biocompatibility were designed. The analysis of the structure – property – function correlation revealed that the incorporation of CH-M as drug carriers did not impaired shape memory properties of 3b-PU matrix and in specified amount of 2.5 and 5 wt% could slightly enhance the shape memory capability of the 3b-PU network and Young Modulus. Additionally, T_m of the PCL switching segments that was tailored to the physiologically relevant range by polymer network composition was not changed after CH-M loading. CH-M after incorporation to the PU matrix revealed sustained drug delivery ability with lower burst release effect. The 3b-PU/CH 2.5% M composites displayed nontoxic behavior what makes the obtained biocomposites a good candidate for minimally invasive surgery systems or shape - memory implants with sustained drug release properties.
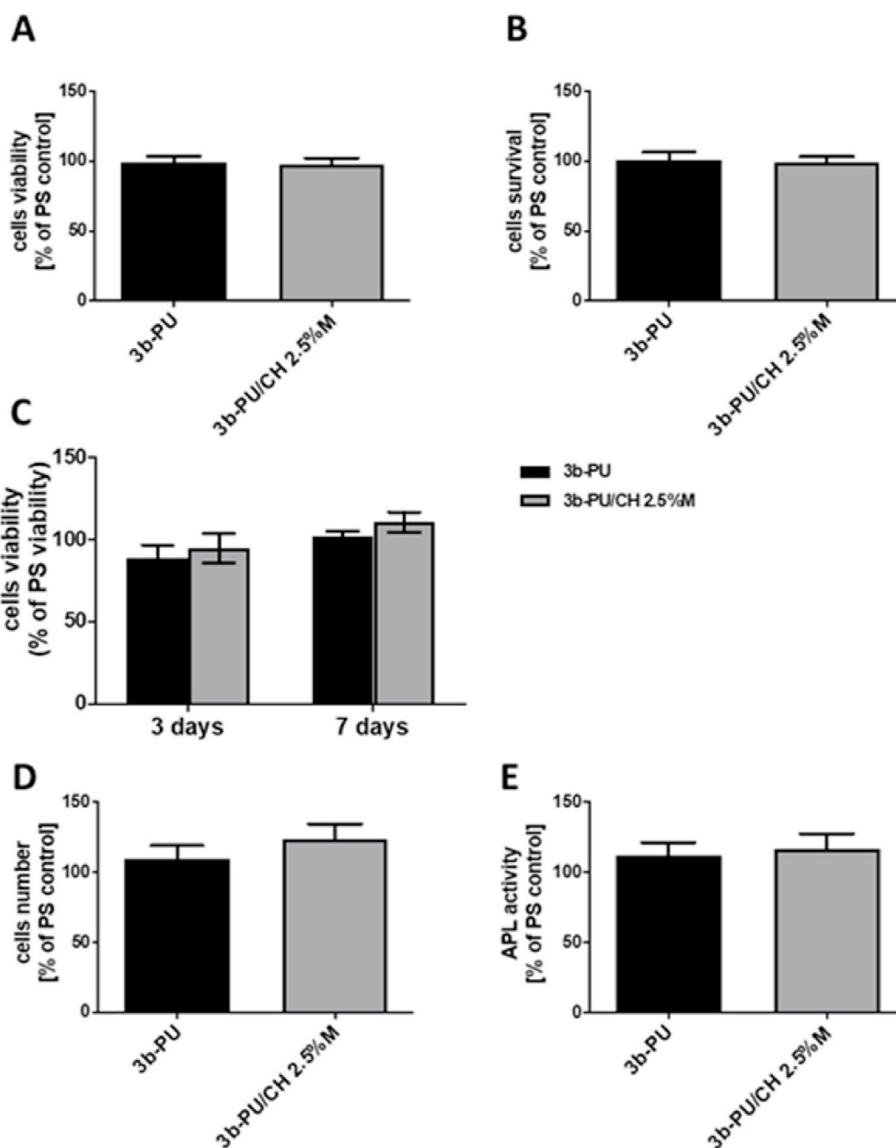
Fig. 7. Biocompatibility studies. A) XTT assessed viability of cells exposed to substances released from the materials; B) number of cells grown in media exposed to samples degradation estimated by quantitative CV staining C) viability of the cells cultured on the materials for 3 and 7 days, tested by XTT method; D) cell counts performed with the PicoGreen® test after 7 days of culture E) ALP activity of cells cultured for 7 days on tested materials. Differences are statistically insignificant.

CRediT authorship contribution statement

Monika Bil: Conceptualization, Investigation, Formal analysis, Analysis, Visualization, Writing - original draft, preparation, Writing - review & editing, Project administration, Funding acquisition. **Piotr Mrówka:** Methodology, Investigation, Formal analysis, Analysis, Visualization, Writing - review & editing. **Dorota Kołbuk- Konieczny:** Investigation, Writing - review & editing. **Wojciech Święszkowski:** Writing - review & editing.

Declaration of competing interest

The authors declare that they have no known competing financial interests or personal relationships that could have appeared to influence the work reported in this paper.

Acknowledgment

Appendix A. Supplementary data

Supplementary data to this article can be found online at https://doi.org/10.1016/j.compscitech.2020.108481.

References

[1] R.A. Perez, Won J-E. Won, J.C. Knowles, H.-W. Kim, Naturally and synthetic smart composite biomaterials for tissue regeneration, Adv. Drug Deliv. Rev. 65 (4) (2013) 471–496.

[2] A. Lendlein, M. Balk, N.A. Tarazona, O.E.C. Gould, Bioperspectives for shape -memory polymers as shape programmable, active materials Biomacromolecules 20 (2019) 3627–3640.

[3] P.S. Kowalski, Ch Bhattacharya, S. Afewerki, R. Langer, Smart biomaterials: recent advances and future directions, ACS Biomater. Sci. Eng. 4 (11) (2018) 3809–3817, https://doi.org/10.1021/acsbiomaterials.8b00889.

[4] W. Zhao, L. Liu, F. Zhang, J. Leng, Y. Liu, Shape memory polymers and their composites in biomedical applications, Mater. Sci. Eng. C 97 (2019) 864–883.

[5] G.D. Mogoşanu, A.M. Grumezescu, Natural and synthetic polymers for wounds and burns dressing, Int. J. Pharm. 463 (2) (2014) 127–136, https://doi.org/10.1016/j.ijpharm.2013.12.015.

[6] M.M. Zagho, E.A. Hussein, A.A. Elzatahry, Recent overviews in functional polymer composites for biomedical applications, Polymers 10 (7) (2018) 739, https://doi.org/10.3390/polym10070739.

[7] W. IV Small, P. Singhal, T.S. Wilson, D.J. Maitland, Biomedical applications of thermally activated shape memory polymers, J. Mater. Chem. 20 (2010) 3356–3366, https://doi.org/10.1039/b923717h.

[8] M. Panahi-Sarmad, M. Abrisham, M. Noroozi, A. Amirkiai, P. Dehghan, V. Goodarzi, B. Zahirid, Deep focusing on the role of microstructures in shape memory properties of polymer composites: a critical review, Eur. Polym. J. 117 (2019) 280–303, https://doi.org/10.1016/j.eurpolymj.2019.05.013.

[9] M. Saenz-Perez, J.M. Laza, J. Garcia-Barrasa, J.L. Vilas, L.M. Leon, Influence of the soft segment nature on the thermomechanical behavior of shape memory polyurethanes, Polym. Eng. Sci. 58 (2) (2018) 238–244.

[10] M. Bil, E. Kijeńska-Gawrońska, E. Głodkowska-Mrówka, A. Manda-Handzlik, P. Mrówka, Design and in vitro evaluation of electrospun shape memory polyurethanes for self-fitting tissue engineering grafts and drug delivery systems Materials, Science and Engineering: Chimia 110 (2020) 110675, https://doi.org/10.1016/j.msec.2020.110675.

[11] L. Shuai, Z. Jun, C. Jianjun, Y. Ming, L. Xuepeng, J. Zhiguo, Biodegradable body temperature-responsive shape memory polyurethanes with self-healing behavior, Polym. Eng. Sci. 59 (2019) E310–E316, https://doi.org/10.1002/pen.25061.

[12] A. Gupta, B.S. Kim, Shape memory polyurethane biocomposites based on toughened polycaprolactone promoted by nano-chitosan, Nanomaterials 9 (2) (2019).

[13] W. Zenga, J. Huanga, X. Hua, W. Xiaoa, M. Rongb, Z. Yuana, Z. Luoa, Ionically cross-linked chitosan microspheres for controlled release of bioactive nerve growth factor International, Journal of Pharmaceutics 421 (2011) 283–290.

[14] S.D. Hua, J. Jiang, L. Kuang, J. Jiang, W. Zheng, H. Liang, Chitosan-based stimuli-responsive nanocarriers for the controlled delivery of hydrophobic pharmaceuticals, Macromolecules 44 (2011) 1298–1302.

[15] F. Kara, E.A. Aksoy, Z. Yuksekdag, N. Hasirci, S. Aksoy, Synthesis and surface modification of polyurethanes with chitosan for antibacterial properties Carbohydrate, Polymers 112 (4) (2014) 39–47.

[16] M. Barikani, K.M. Zia, I.A. Bhatti, M. Zuber, H.N. Bhatti, Molecular engineering and properties of chitin based shape memory polyurethanes Carbohydrate, Polymers 74 (3) (2008) 621–626.

[17] K. Kawaguchi, M. Iijima, H. Miyakawa, M. Ohta, T. Muguruma, K. Endo, F. Nakazawa, I. Mizoguchi, Effects of chitosan fiber addition on the properties of polyurethane with thermo-responsive shape memory, J. Biomed. Mater. Res. Part B 105B (2017) 1151–1156.

[18] A. Saralegi, S.C.M. Fernandes, A. Alonso-Varona, T. Teodoro Palomares, E. J. Foster, Ch Weder, A. Eceiza, M.A. Corcuera, Shape-memory bionanocomposites based on chitin nanocrystals and thermoplastic polyurethane with a highly crystalline soft segment, Biomacromolecules 14 (2013) 4475–4482.

[19] E. Szymanska, K. Winnicka, M. Muśko, Preparation of chitosan microspheres by emulsion/polymerization method using tripolyphosphate (TPP) and glutaraldehyde (GL), Farm. Pol. 66 (4) (2010) 238–242.

[20] J. Dulnik, P. Denis, P. Sajkiewicz, D. Kołbuk, E. Choińska, Biodegradation of bicomponent PCL/gelatin and PCL/collagen nanofibers electrospun from alternative solvent system, Polym. Degrad. Stabil. 130 (2016) 10–21.

[21] P. Mrówka, J. Kozakiewicz, A. Jurkowska, E. Sienkiewicz, J. Przybylski, Z. Lewandowski, J. Przybylski, M. Lewandowska-Szumieł, Moisture-cured silicone-urethanes-candidate materials for tissue engineering: a biocompatibility study in vitro, J. Biomed. Mater. Res. 94 (1) (2010) 71–83.

[22] T. Mu, L. Liu, X. Lan, Y. Yanju Liu, J. Leng, Shape memory polymers for composites Composites, Sci. Technol. 160 (2018) 169–198.

[23] D.R. Bhumkar, V.B. Pokharkar, Studies on effect of pH on cross-linking of Chitosan with sodium tripolyphosphate: a technical note, AAPS PharmSciTech 7 (2) (2006) E50.

[24] N.R. Kildeeva, P.A. Perminov, L.V. Vladimirov, V.V. Novikov, S.N. Mikhailov, About mechanism of chitosan cross-linking with glutaraldehyde Russian, Journal of Bioorganic Chemistry 35 (3) (2009) 360–369.

[25] C. Guignot, N. Betz, B. Legendre, A. Leomel, N. Yagoubi, Influence of filming process on macromolecular structure and organization of a medical segmented polyurethane, J. Appl. Polym. Sci. 85 (2002) 1970–1979.

[26] G. Socrates, Infrared and Raman Characteristic Group Frequencies: Tables and Charts, third ed., John Wiley & Sons, 2001, pp. 153–154.

[27] J. Mattia, P. Painter, A comparison of hydrogen bonding and order in a polyurethane and poly(urethane-urea) and their blends with poly(ethylene glycol), Macromolecules 40 (2007) 1546–1554.

[28] A. Bossion, New Challenges in the Synthesis of Non-isocyanate Polyurethanes. Polymers, Université de Bordeaux; Universidad del País Vasco, 2018. English. ffNNT: 2018BORD0360ff. fftel-01998058f.

[29] N. Arshad, K.M. Zia, F. Jabeen, M.N. Anjuma, N. Akrama, M. Zuber, Synthesis, characterization of novel chitosan based water dispersible polyurethanes and their potential deployment as antibacterial textile finish in the polymers, Int. J. Biol. Macromol. 111 (2018) 485–492.

[30] T. Vieira, J. Carvalho, S.J.P. Borges, C. Henriques, Synthesis, electrospinning and in vitro test of a new biodegradable gelatin-based poly (ester urethane urea) for soft tissue engineering, Eur. Polym. J. 103 (2018) 271–281.

[31] Shaojun Chen, Jinlian Hu, Haitao Zhuo, Properties and mechanism of two-way shape memory polyurethane composites, Compos. Sci. Technol. 70 (2010) 1437–1443.

[32] R.C.M. Dias, A.M. Góes, R. Serakides, E. Ayres, R.L. Oréfice, Porous biodegradable polyurethane nanocomposites: preparation, characterization, and biocompatibility tests, Mater. Res. 13 (2) (2010) 211–218.

[33] M. Ioelovich, Crystallinity and hydrophility of chitin and chitosan, J. Chem. 3 (3) (2014) 7–14.

[34] Z. Ren, L. Dong, Y. Yang, Dynamic mechanical and thermal properties of plasticized poly (lactic acid), J. Appl. Polym. Sci. 101 (3) (2006) 1583–1590.

[35] P.L. Ritger, N.A. Peppas, A simple equation for description of solute release II. Fickian and anomalous release from swellable devices, J. Contr. Release 5 (1987) 37–42.

[36] J.M. Unagolla, A.C. Jayasuriya, Drug transport mechanisms and in vitro release kinetics of vancomycin encapsulated chitosan-alginate polyelectrolyte microparticles as a controlled drug delivery system, Eur. J. Pharmaceut. Sci. 114 (2018) 199–209, https://doi.org/10.1016/j.ejps.2017.12.012.

[37] Y. Fu, W.J. Kao, Drug release kinetics and transport mechanisms of nondegradable and degradable polymeric delivery systems, Expet Opin. Drug Deliv. 7 (4) (2010) 429–444, https://doi.org/10.1517/17425241003602259.